

OPEN ACCESS

EDITED BY Giovanni Porta, University of Insubria, Italy

REVIEWED BY
Jinghua Lu,
National Institute of Allergy and Infectious
Diseases (NIH), United States
Yinglong Miao,
University of North Carolina at Chapel Hill,
United States

*CORRESPONDENCE
Andrea Cavalli

andrea.cavalli@irb.usi.ch
Jacopo Sgrignani

jacopo.sgrignani@irb.usi.ch

[†]These authors share first authorship

RECEIVED 20 May 2025 ACCEPTED 13 August 2025 PUBLISHED 12 September 2025

CITATION

Sgrignani J, Buscarini S, Locatelli P, Guerra C, Furlan A, Chen Y, Zoppi G and Cavalli A (2025) Al-assisted design of ligands for lipocalin-2. Front. Immunol. 16:1631868. doi: 10.3389/fimmu.2025.1631868

COPYRIGHT

© 2025 Sgrignani, Buscarini, Locatelli, Guerra, Furlan, Chen, Zoppi and Cavalli. This is an open-access article distributed under the terms of the Creative Commons Attribution License (CC BY). The use, distribution or reproduction in other forums is permitted, provided the original author(s) and the copyright owner(s) are credited and that the original publication in this journal is cited, in accordance with accepted academic practice. No use, distribution or reproduction is permitted which does not comply with these terms.

Al-assisted design of ligands for lipocalin-2

Jacopo Sgrignani^{1*†}, Sara Buscarini^{1†}, Patrizia Locatelli¹, Concetta Guerra¹, Alberto Furlan¹, Yingyi Chen¹, Giada Zoppi¹ and Andrea Cavalli^{1,2*}

¹Institute for Research in Biomedicine (IRB), Università della Svizzera Italiana (USI), Bellinzona, Switzerland, ²Swiss Institute of Bioinformatics (SIB), Lausanne, Switzerland

Introduction: Lipocalin-2 (LCN2) is an acute-phase glycoprotein whose upregulation is associated with blood-brain-barrier breakdown and neuroinflammation, making it a potential diagnostic and therapeutic target.

Methods: We developed an end-to-end, Al-guided workflow to design de-novo miniproteins targeting LCN2. Backbone scaffolds were generated using RFdiffusion, sequences optimized with ProteinMPNN, and candidates filtered in silico based on AlphaFold2 confidence metrics (mean interface pAE < 10) and binding free energy predicted by Prodigy. From an initial library of 10,000 designs, five candidates were expressed and purified from E. coli. Binding affinities were assessed using biolayer interferometry (BLI), and structural interactions were analyzed via computational modeling.

Results: BLI identified MiniP-2 as the lead construct, exhibiting a dissociation constant (Kd) of 4.2 nM. Structural modeling indicated that binding is primarily mediated by backbone hydrogen bonds, complemented by a stabilizing salt bridge between Arg37 of MiniP-2 and Asp97 of LCN2. Surface plasmon resonance (SPR) competition experiments demonstrated that MiniP-2 inhibits LCN2 binding to MMP-9, highlighting its potential to interfere with pathological LCN2 interactions. **Discussion:** These results demonstrate that a fully computational generative workflow can yield nanomolar LCN2 binders in a single design—build—test cycle. MiniP-2 represents a promising starting point for affinity maturation, structural studies, and in vivo evaluation as an imaging probe or antagonist of LCN2-mediated signaling.

KEYWORDS

artificial intelligence, minibinders, lipocalin 2, protein design, binding assays

Introduction

Lipocalin-2 (LCN2) - also known as neutrophil gelatinase-associated lipocalin, siderocalin or 24p3 - is an acute-phase glycoprotein rapidly upregulated during infection and sterile inflammation (1). Like other members of the lipocalin family, LCN2 adopts the canonical eight-stranded $\beta\text{-barrel},$ which allows it to bind bacterial siderophores and

sequester iron, thereby acting as a key first-line defense mechanism against pathogens (Figure 1) (1, 3).

The interaction between LCN2 and its receptor NGALR plays a significant role in various cellular processes and is implicated in several pathological conditions. In particular, binding to NGALR amplifies pro-inflammatory cytokine release (4, 5) and, when over-expressed by reactive glia, contributes to neurotoxicity in several central nervous system (CNS) disorders (6).

LCN2 also forms stable heterodimers with MMP-9, a zinc-dependent matrix metalloproteinase (7, 8). This interaction stabilizes MMP-9, preventing its degradation. As a key enzyme for extracellular matrix remodeling, MMP-9 plays a critical role in breaking down extracellular matrix components. Excessive MMP-9 activity disrupts the integrity of the Blood-Brain Barrier (BBB), contributing to the development of neurodegenerative diseases such as Alzheimer's and Parkinson's (9). Dysregulation of MMP-9 has also been linked to ischemia, trauma, neurodegenerative disorders (10, 11) and brain tumors (12).

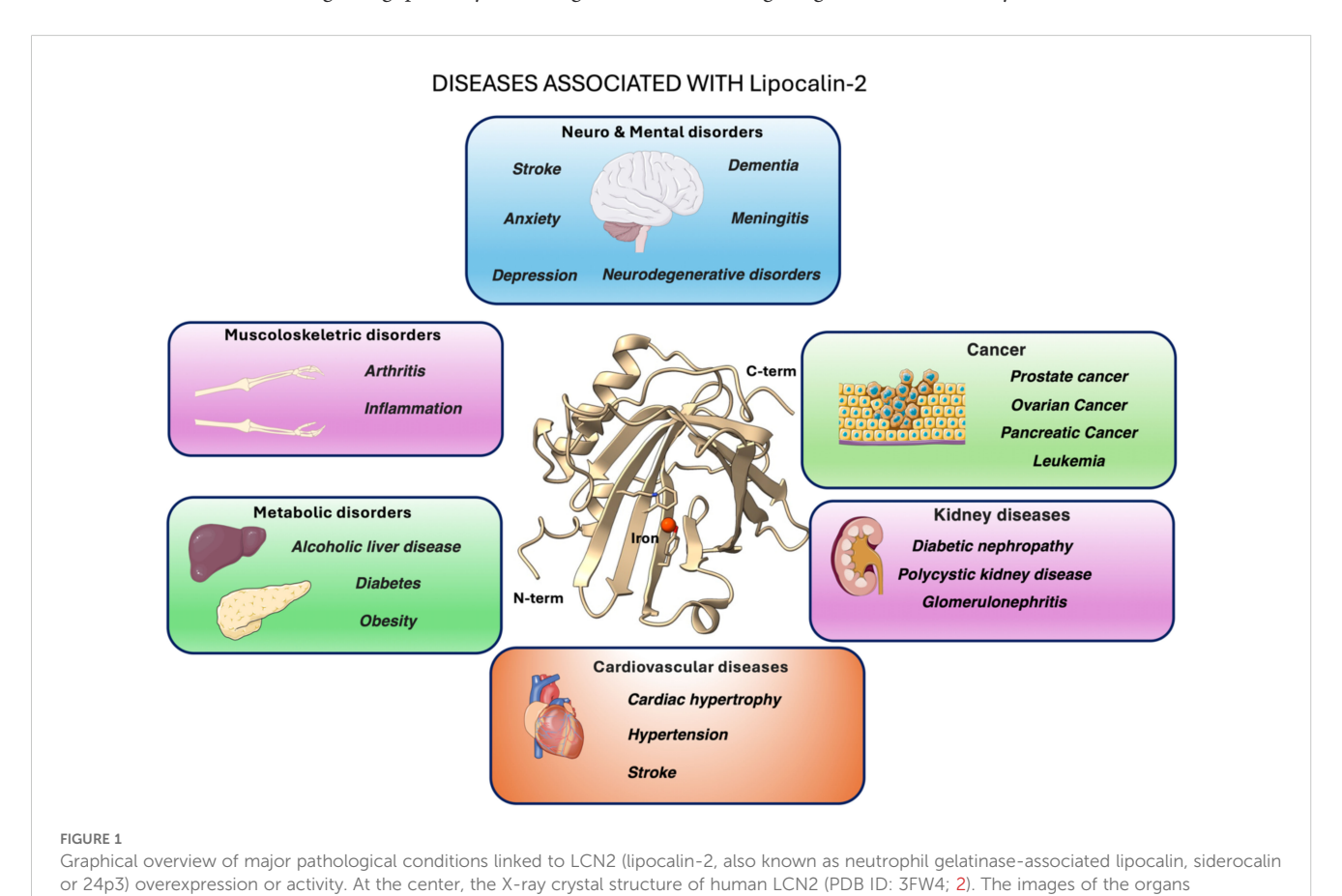
Despite LCN2's central role in neuroinflammation, no blood-brain barrier (BBB) permeable ligands exist that can either block the LCN2-NGALR signaling or disrupt the LCN2-MMP-9 heterodimer - both promising therapeutic strategies. Current therapeutic approaches against LCN2-driven pathogenic mechanisms aim to reduce its expression or secretion, enhance its degradation, block its activity with neutralizing antibodies, inhibit receptor binding, or interfere with downstream signaling pathways. Among small-

creativecommons.org/licenses/by/4.0/).

molecule approaches, promising outcomes have been reported for the proteasome inhibitor bortezomib (13), which reduces LCN2 transcription, and for the autophagy activator Torin 1, which decreases LCN2 protein levels (14). Antibody-based therapies represent another viable strategy to block LCN2 function and signaling. However, their large molecular weight severely limits blood-brain barrier (BBB) permeability, reducing their effectiveness in neurological applications. To overcome these limitations, we propose that engineered miniprotein binders (typically proteins with a mass below 10 kDa) with high affinity for LCN2 could serve as a versatile and BBB-compatible therapeutic platform. Proteinprotein interaction (PPI) modulators are generally classified as small molecules, peptides, and antibodies (15). While small molecules offer advantages such as oral bioavailability and stability, peptides or antibodies are often more effective at disrupting PPIs, especially those involving large, flat interaction interfaces lacking well-defined binding pockets.

Recent advances in AI-driven protein design - pioneered by the Baker laboratory – have enabled the *de novo* generation of miniproteins (10–15 kDa) capable of binding targets of interest (16–19).

Building on these advances, we established an AI-guided pipeline to design *de novo* miniproteins that block the LCN2 interfaces involved in NGALR and MMP-9 binding. Using this approach, we computationally designed, expressed in E. coli, and biophysically characterized five AI-generated candidates, identifying a lead binder with single-digit nanomolar affinity for LCN2.



represented in the pictures were adapted from Servier Medical Art (https://smart.servier.com/), licensed under CC BY 4.0 (https://smart.servier.com/),

Methods

General reagents and buffers

All chemicals were analytical grade. Recombinant human LCN2 was produced and purified by GenScript. The MMP-9 protein used in SPR studies was acquired from antibodies.com (code A331071-50). Twin-Strep-tag magnetic beads, Buffer W and Buffer BXT were from IBA LifeSciences. Dynamic-light-scattering (DLS) and nano-DSF assays were carried out in phosphate-buffered saline (PBS; 20 mM sodium-phosphate, 150 mM NaCl, pH 7.4). All other solutions are described below.

Miniprotein computational design

The generation of miniproteins to bind LCN2 was carried out using the procedure described by Baker and co-workers (20) (https://github.com/RosettaCommons/RFdiffusion). The crystal structure of LCN2 (PDB ID: 1DFV) was selected as template structure (21). Following the protocol author's suggestion, we generated 10,000 backbone scaffolds using RF diffusion (20) and subsequently designed 10,000 sequences with ProteinMPNN (22) to create LCN2 binders. Finally, the ability of the generated sequences to correctly fold and to bind the target was evaluated using AlphaFold2 (AF2) (23).

For each model we recorded the mean pLDDT and the interface predicted aligned-error (pAE_interface). Designs with pAE_interface<10 were retained, yielding 1,184 candidates.

Next, to select the five most promising binders, we estimated the LCN2-binder affinity with PRODIGY, a contact-based predictor of protein-protein affinity (24). Finally, the five proteins reporting the most negative ΔG were expressed and purified.

Alanine scanning with DrugScorePPI server

To identify the molecular determinants of the MinP-2/LCN2 interaction, we analyzed the AF2-predicted complex structure using the DrugScorePPI server (25).

Assessment of protein expression

The DNA sequences encoding the five select miniproteins were synthesized and cloned by GenScript into the pET30b plasmid, incorporating a Twin-Strep tag for purification. *E. coli* BL21 (DE3) pLysS cells were transformed with the plasmids and plated onto five separate LB-agar plates. Following overnight incubation, colonies that successfully incorporated the plasmids were selected.

Before starting the protein production and purification, we assessed miniprotein expression in *E.coli* BL21 (DE3) pLysS cells analyzing induced and not induced cultures by Western-Blot (WB).

Samples (20 μ l) from both IPTG-induced and non-induced cultures were mixed with 20 μ l of sample buffer containing Tris-Glycine SDS and a sample reducing agent. From these prepared

stocks, 20 µl were loaded onto the gel. Following electrophoresis, the SDS-PAGE gel was transferred into a membrane. After the transfer, the membrane was activated with methanol and subsequently washed with Tris-buffered saline containing 0. 1% Tween[®] 20 (TBST). Following the washing step, blocking was performed with TBST and milk to prevent nonspecific binding. Subsequently, another washing step was conducted, and the primary antibody (IBA Lifesciences 2-1507-001; Anti-Strep) was added.

The next day, the primary antibody was removed, and the secondary antibody (anti-mouse IgG1 conjugated with horseradish peroxidase (HRP)) was applied. After the incubation step, another washings step was performed, and reagents were added to develop the Western Blot.

Miniprotein expression and purification

Following positive WB results, a bacterial preculture was prepared by inoculating a single colony into 7 mL of Luria-Bertani (LB) medium supplemented with chloramphenicol and kanamycin, and incubated at 37 °C to promote bacterial growth.

Subsequently, 1 mL of the preculture was inoculated into 200 mL of LB medium and incubated at 37 °C until the culture reached an OD_{600} of 0.6. Protein expression was then induced by adding IPTG to a final concentration of 1 mM. After overnight incubation, bacterial cells were resuspended in a PBS added with two tablets of protease inhibitor (cOmplete $^{\rm TM}$, Mini, EDTA-free Protease Inhibitor Cocktail) and lysed by sonication. The lysate was then filtered through a 0.22 μ m membrane to remove debris before purification.

Strep-tag purification was performed using magnetic beads (IBA LifeSciences). Beads were washed with 1x Buffer W, followed by an incubation step to allow protein binding. After additional washing, elution was carried out using 1X Buffer BXT, yielding purified miniproteins in the eluate. Residual biotin in the elution buffer was removed by dialysis. Purity was verified by SDS-PAGE.

Dynamic-light scattering and nano-DSF

The size distribution and thermal stability of all miniproteins were analyzed using a Prometheus Panta (NanoTemper). Measurements were performed in triplicate, with miniproteins directly loaded into capillaries at concentrations of 0.32, 0.22, 0.18, 0.10, and 0.2 mg/mL for MinP-1 to MinP-5, respectively.

Bio-layer interferometry

Interactions between the designed miniproteins and LCN2 were analyzed using biolayer interferometry (BLI). LCN2 was immobilized by His-tag on BLI sensors Octet Ni-NTA (NTA) Biosensors using a concentration of $5\mu g/ml$. All the experiments were run using a Octet Rs instrument. All miniproteins were tested at a concentration of $4\,\mu M$. For MinP-2, which showed clear binding, titration experiments were performed at 1000, 500, 250, 125, 62.5, 31.2, and 15.6 nM. The signal from a reference sensor without immobilized protein was subtracted to

remove background noise and aspecific binding. Association and dissociation phases were 300 s each, and data were fitted globally with a 1:1 and 2:1 binding models in the Octet Analysis software.

MMP-9/LCN2 interaction a single concentration of 200 nM LCN2 alone or mixed with an equimolar concentration of MinP-2 was injected for 45s followed by 60s of dissociation.

Surface plasmon resonance

SPR experiments were performed using a Biacore 8K system (Cytiva, Marlborough, MA, USA). MinP-2 dissolved in 10 mM sodium acetate (pH 4.5) at a concentration of 2 μ M was immobilized via amine coupling onto a CM5 sensor chip (GE Healthcare, Chicago, IL, USA). MMP-9 was immobilized using the same procedure using protein concentration of 300 nM.

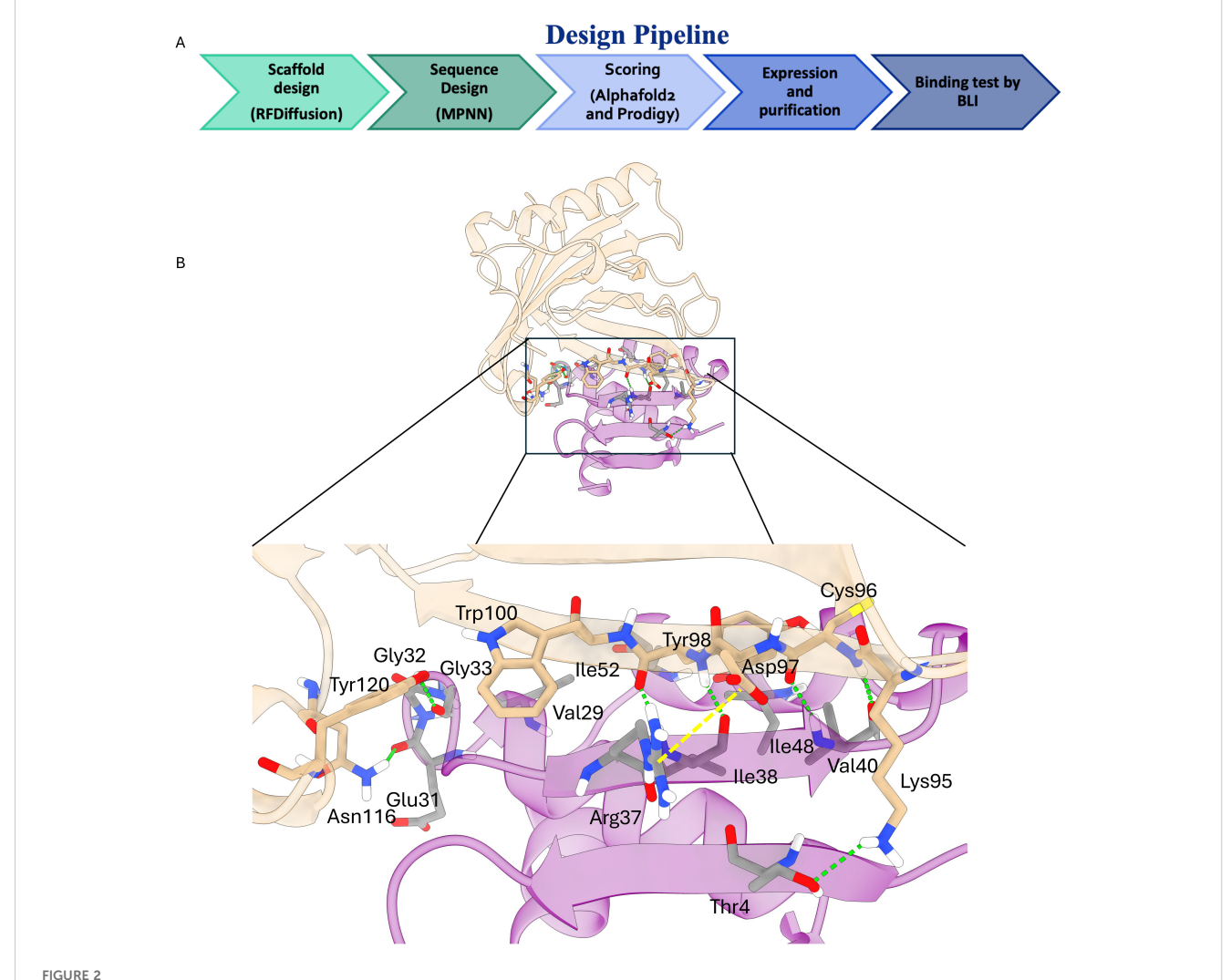
Five concentrations of LCN2 (7.8, 15.6, 31.2, 62.5, and 125 nM) were injected over the immobilized MinP-2 at a flow rate of 30 $\mu L/min$. The contact time for each injection was 120 s, while the dissociation phase was run for 600 s. All the experiments were performed at 25 °C. Following blank subtraction, the binding data were fitted and analyzed using Biacore Insights Evaluation Software v. 5.0.18. In the case of the

Results

In silico miniprotein design pipeline and candidate selection

In the initial phase of the project, we applied the computational pipeline originally proposed by Baker and colleagues (20). Starting from 10,000 backbone scaffolds generated with RFdiffusion, a single ProteinMPNN sequence was designed for each scaffold. AlphaFold2 rescoring retained 1,184 binders with a pAE_interaction score below 10 - a threshold shown to enrich for functional hits (26) (Figure 2A) 1S.

However, expressing and purifying such a large number of proteins is impractical. To overcome this limitation, we applied a consensus scoring approach to refine the selection. Specifically, all



(A) Schematic representation of the applied computational pipeline. (B) Key molecular interactions driving the binding of MinP-2 (magenta cartoons) to LCN2 (white cartoons). The key interactions highlighted by the black box are shown in detail in the lower panel. Hydrogen bonds are shown as green dotted lines with the salt bridge as a dotted yellow line.

1,184 candidates were re-ranked with the contact-based affinity predictor PRODIGY (24), and the five miniproteins with the most negative predicted ΔG were selected for expression (Table 1, Supplementary Figure S3).

Expression, purification and biophysical characterization of AI designed miniproteins

Given that the proteins were designed by AI, before large-scale production we assessed the expression of the five constructs in *E. coli* by WB (Supplementary Figure S1). This preliminary analysis confirmed that all proteins were expressed, although MinP-2 and MinP-3 showed lower expression levels. Consequently, we proceeded with large-scale expression and purification of all five constructs. Purification was performed using magnetic beads functionalized with a modified streptavidin (Strep-Tactin[®]XT, IBA Lifesciences), yielding highly pure proteins in sufficient quantities for subsequent biophysical characterization (Supplementary Figure S2).

Before evaluating LCN2 binding, all purified constructs were characterized for size distribution via dynamic light scattering (DLS) and thermal stability via nanoDSF. DLS analysis revealed that all constructs - except MinP-4 - were monodisperse with an apparent hydrodynamic radius of approximately 2 nm, consistent with their predicted molecular weight and structural models (Figures 3A–E, 4A–E). In contrast, MinP-4 showed a polydispersity index (PDI) of 0.38, indicative of aggregation. Thermal stability analysis by nanoDSF showed that only MinP-5 displayed a clear melting temperature (Tm at 46.8 °C). This is notably lower than the high thermal stability (Tm > 90 °C) reported for some AI-designed miniprotein binders by Baker and colleagues (16).

Binding of miniproteins to LCN2 investigated by BLI and SPR

Preliminary binding assays at 4 μ M were performed to evaluate the interaction of the five miniproteins with LCN2. Among them, MinP-2 emerged as the most promising binder (Figure 5A), whereas the other constructs displayed only weak or negligible binding.

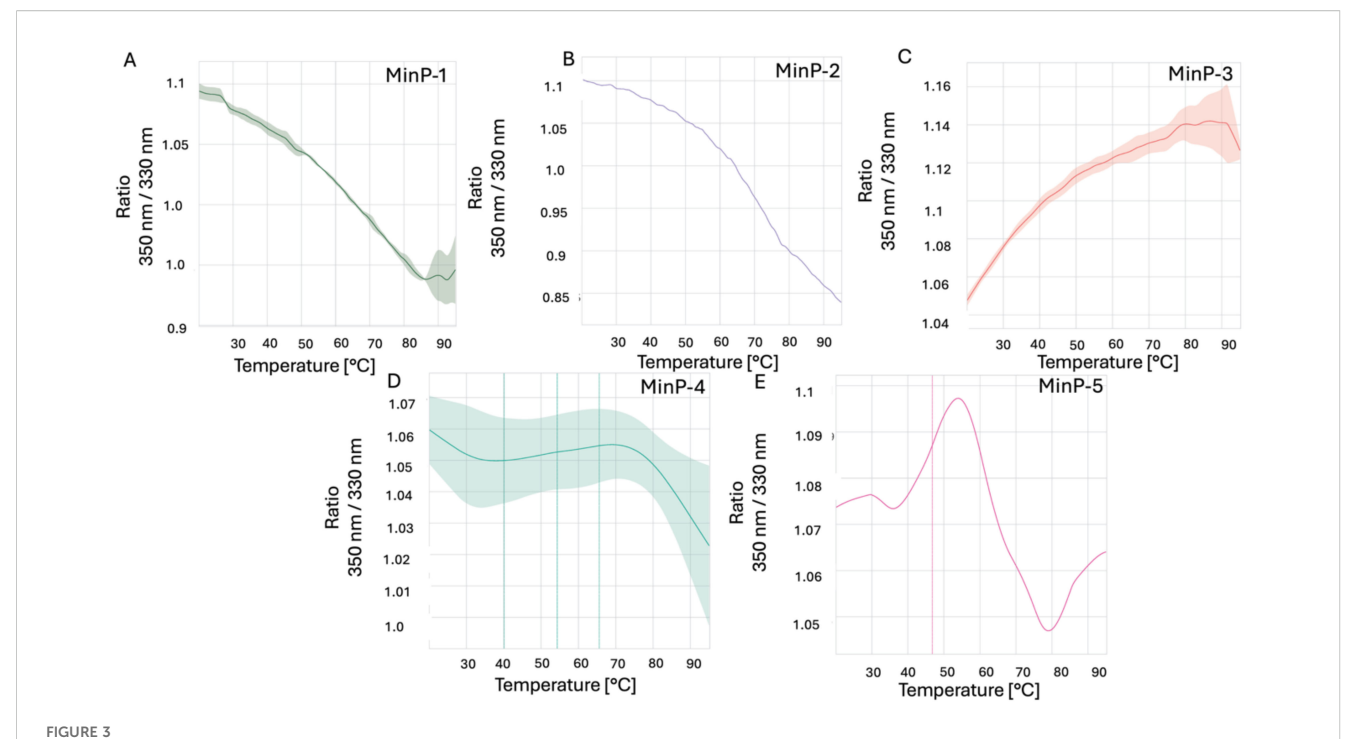
Therefore, to fully characterized affinity and kinetics of the LCN2-MinP-2 interaction we performed a titration across seven concentrations (Figure 5B). This experiment showed that MinP2 strongly binds LCN2, with two dissociation constants (Kd1 = 0.7 and Kd2 = 35 nM) obtained using a 2:1 heterogeneous model. The requirement for a 2:1 model may stem from surface crowding on the sensor, partially blocking MinP-2 binding sites and resulting in a secondary, lower-affinity interaction.

To verify if the immobilization strategy used in the BLI experiment could be the source of the 2:1 binding, we performed surface plasmon resonance (SPR) experiments (Figure 5C). In this case, confirming our hypothesis about the influence of the immobilization strategy on the results, the data were best fitted with a 1:1 model, yielding a Kd for the LCN2/MinP-2 complex of 4.2 nM.

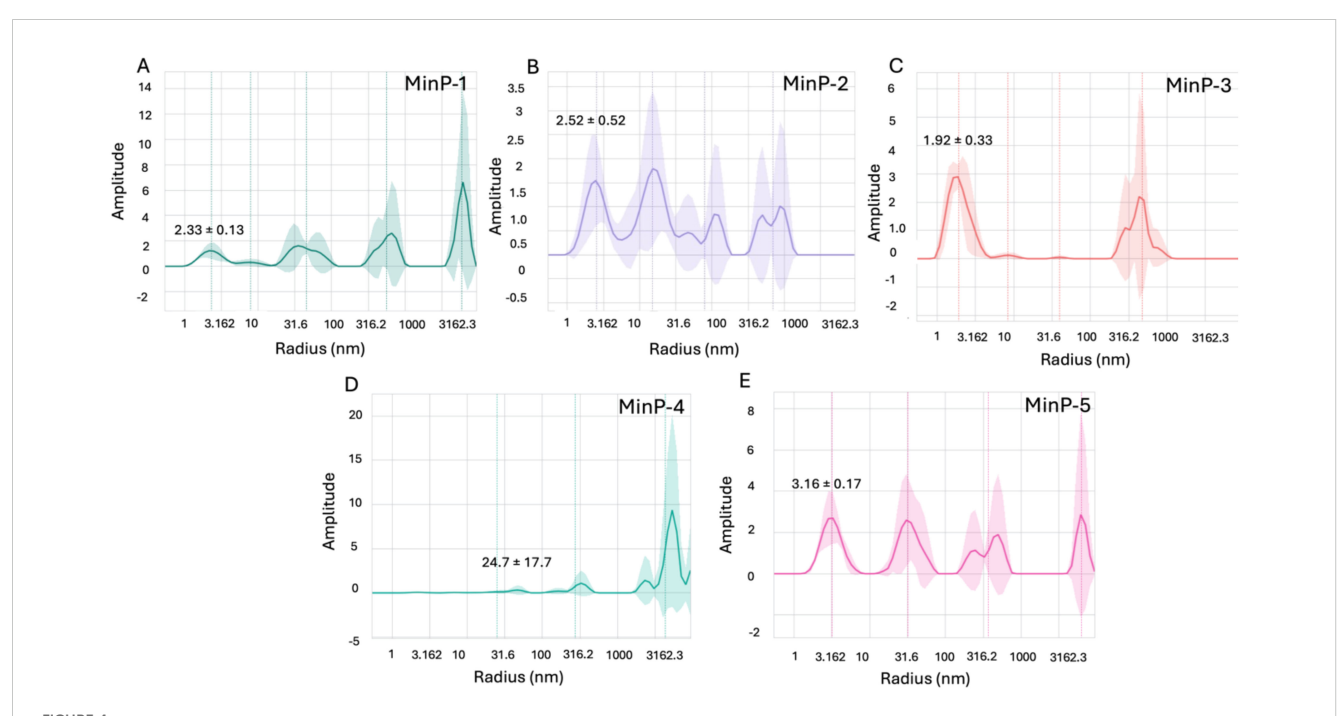
five miniproteins selected for further studies after computational the for predicted ∆G Aminoacidic sequences and

Name	Sequence	Predicted ∆G (kcal/mol)	Pae_ interaction
ıP-1	KKKVAVVVVRKTPEEAKAGFEEAKPNVELVASILSEDFEVETLAVTEEEYDEVLEKYDFVVRVYKMDLESAKISAKLIREHIKEIVK	-11.0	4.05
ъР-2	MSKATVYDVSTGKTYEVSLEDAKKLASYAVYEGGYPLRISVAPEDTKAILDAIKNTSKEKAEEGKKLLEELN	-12.7	4.08
лР-3	MKRVEIKALDNVENANAIAEVLKSHGIPVEVKEVSPDLKEVTSEAVVSEELAEKIKESLIELAKKLGPVGPIHISISDV	-11.7	4.20
nP-4	MTVNVTITANSDGWISIKATTDETAKLAVEIAKEYLPTKSFDETAEATINALATKKGGTATITKSGNTYYATIT	-13.4	4.22
nP-5	MLKELEEKIFKENPEVKKILEKLSKALGVKVEVSVEKVDGVYRFVLRVDVKDHPKVNMKILSELGLKLQLAAGEELTKLL	-12.3	4.22

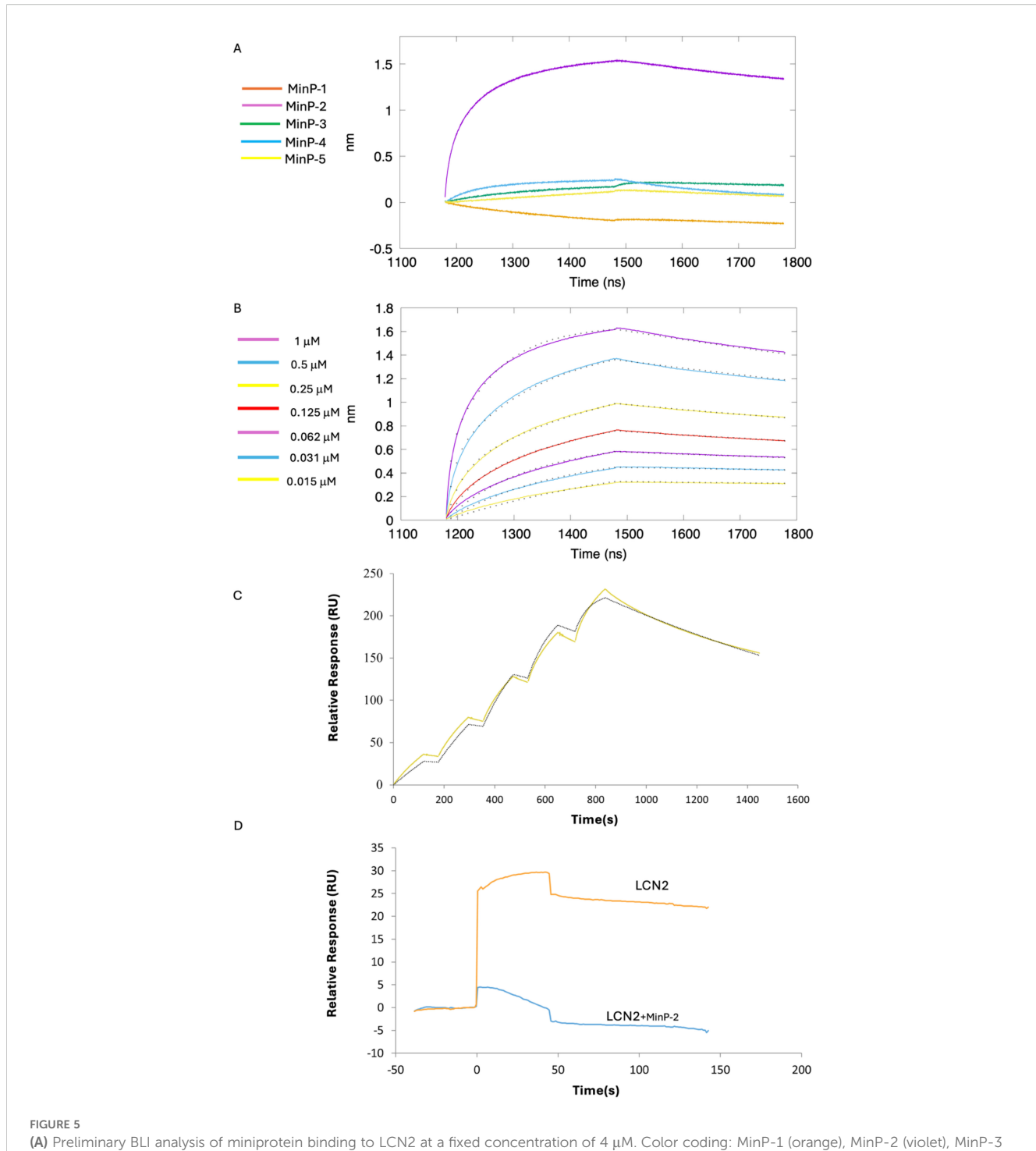
he ligands are ordered by pae_interaction score



Results of nanoDSF experiments. The ratio of fluorescence intensity measured at 350 nm to the fluorescence intensity measured at 330 nm at different increasing temperatures for the five designed miniproteins This value reflects changes in the environment of tryptophan (Trp) residues within the protein making possible to monitor its stability at different temperatures. Data for Min-P1, Min-P2, Min-P3, Min-P4 and Min-P5, are shown in panels A–E respectively.



Results of DLS experiments. The DLS plots reflect the intensity of scattered light, which is proportional to the sixth power of particle size (\propto size⁶). Thus, larger particles appear overrepresented in intensity despite being fewer in number. For example, the ~2 nm peak contains ~2×10⁶ more particles than the ~40 nm peak, and ~2×10¹² more than the ~400 nm peak, even though the peaks may appear similar in height. Data for Min-P1, Min-P2, Min-P3, Min-P4 and Min-P5, are shown in panels **A–E** respectively.



(A) Preliminary BLI analysis of miniprotein binding to LCN2 at a fixed concentration of 4 μ M. Color coding: MinP-1 (orange), MinP-2 (violet), MinP-3 (green), MinP-4 (light blue), MinP-5 (yellow). (B) BLI titration curves of MinP-2 binding to LCN2 across seven concentrations, from top to bottom: 1 μ M (violet), 0.5 μ M (light blue), 0.25 μ M (yellow), 0.125 μ M (red), 0.0625 μ M (violet), 0.0312 μ M (light blue), and 0.0156 μ M (yellow). Experimental data are shown as colored lines, with corresponding fitted values indicated by black dots. (C) Results of the LCN2/MinP-2 binding experiments by SPR. Sensogram is shown as a continuous yellow line, while fitted data are indicated as black dotted line. (D) Results of the SPR competition assay showing that MinP-2 inhibits MMP-9/LCN-2 binding.

Structural insight into the LCN2/MinP-2 interface

To better understand the molecular determinants of the LCN2/MinP-2 interaction, we performed a computational alanine scanning analysis on the structure AlphaFold2-predicted complex using the

DrugScorePPI server. The results (Supplementary Tables S1-2) and visual inspection of the interface (Figure 2B) reveled that binding is determined by multiple intermolecular interactions, notably: (i) backbone hydrogen bonds between LCN2 residues Cys96, Asp97, and Tyr98 and the MinP-2 residues Ile38 and Val40 forming a short antiparallel β -augmentation interface; (ii) additional hydrogen bonds

between LCN2 Lys95, Asn116, and Tyr120 with MinP-2 residues Thr4, Glu31, and Gly33; and (iii) a salt bridge between Arg37 of MinP-2 and Asp97 of LCN2. Taken together, these interactions rationalize the observed low-nanomolar affinity.

Assessing the inhibition of the MMP-9/LCN2 interaction by SPR

To evaluate whether MinP-2 can prevent the interaction between MMP-9 and LCN2, we performed an SPR experiment in which LCN2 - alone or in presence of an equimolar (200 nM) concentration of MinP-2 - was injected over immobilized MMP-9. This experiment (Figure 5D) demonstrated that MinP-2 effectively LCN2/MMp-9 interaction.

Discussion

Lipocalin-2 (LCN2) drives, among other effects, BBB breakdown and neuroinflammation through interactions with its partners NGALR and MMP-9. However, no ligands with a molecular weight smaller than an antibody are currently available to block these interactions. Here we show that a 12-kDa miniprotein (MinP-2), generated in a single AI-guided cycle, binds LCN2 with single-digit nanomolar affinity (Kd 4.2 nM). This affinity is comparable to that observed for monoclonal antibodies, but achieved with a 10-fold smaller molecule. Our strategy, incorporating a contact-based scoring approach, demonstrates that consensus rescoring with AlphaFold2 and PRODIGY facilitates the identification of true binders among a large number of AI generated miniproteins, thereby reducing experimental efforts in protein purification and binding tests. All five selected miniproteins were successfully expressed in E. coli, and four were monodisperse and thermostable.

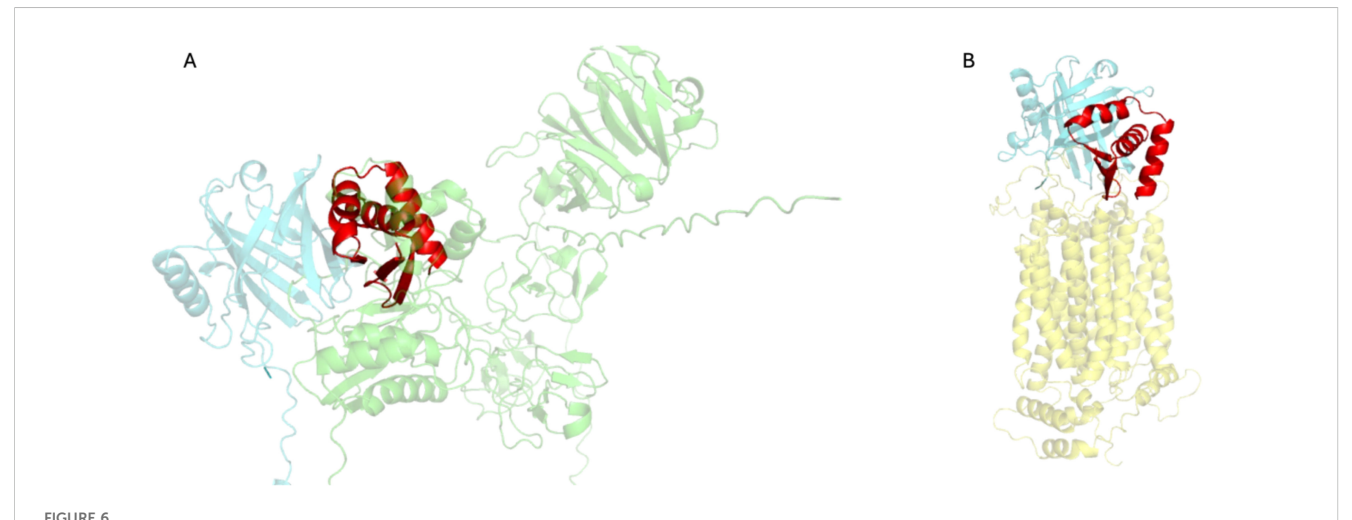
In fact, quality control analyses performed using DLS and nanoDSF revealed that, with the exception of MinP-5, all proteins are thermally stable and predominantly monomeric in PBS at a concentration of ~10–12 μ M, consistent with previous reports (27). However, MinP-4 exhibited a tendency toward aggregation, representing an exception to this general behavior.

From preliminary BLI experiments, MinP-2, a designed miniprotein, emerged as a promising candidate, demonstrating significant interaction with LCN2 and warranting further detailed characterization. Binding analysis revealed that MinP-2 interacts with LCN2 with a dissociation constant (Kd) in the low nanomolar range of 4.2 nM, underscoring its potential for future applications in therapeutic or diagnostic settings.

When comparing the success rate of our protocol to previous studies, the identification of a strong LCN2 binder among just 5 miniproteins is notable. For many target - such as TrkA, EGFR, InsulinR, CD3 (28) – hit rates are below 1% when a 400 nM affinity threshold, with 15,000 and 100,000 candidates tested. However, we acknowledge that the high success rate observed in our study might be influenced by the specific nature of LCN2 as a target. More extensive benchmarks are required to fully evaluate the impact of incorporating physical or contact-based scores into the binder selection process.

To better understand MinP-2's binding mode, we examined AlphaFold2 models of the LCN2 MinP-2 complex. The analysis indicates that affinity is mediated by a short β -augmentation segment: backbone-to-backbone hydrogen bonds form between LCN2 and MinP-2 residues, creating a continuous strand that anchors the miniprotein to its target complemented by additional hydrogen bonds and a salt bridge between Arg37 of MinP-2 and Asp97 of LCN2.

To explore whether MinP-2 can block interactions with MMP-9 and NGALR, we predicted the structures of the respective complexes using AlphaFold3. The result of these calculations (Figure 6) suggested that MinP-2 has the potentiality to hinder their interaction with LCN2.



Complexes of LCN2 with MMP-9 and NGALR predicted by AlphaFold3, superimposed to LCN2/MinP-2. (A) Model of the LCN2 (aquamarine)-MMP-9 (green) complex, overlaid MinP-2 (red) structure. (B) Model of the LCN2 (aquamarine)-NGALR (yellow) complex, overlaid with the LCN2/MinP-2 (red). The images were produced by superimposing the LCN2 structure found in the MMP-9/LCN2 and NGALR/LCN2 complexes onto the LCN2 structure from the LCN2/MinP-2 complex. To enhance clarity, only the LCN2 structures from the MMP-9/LCN2 and NGALR/LCN2 complexes are displayed.

MMP-9 can be readily expressed, purified, and is commercially available. Therefore, to experimentally confirm our hypothesis, we carried out a competitive SPR experiments (Figure 4D). The results confirmed that MinP-2 can prevent the MMP-9/LCN2 interaction. Differently, NGALR is a membrane protein which expression and purification in a binding-competent form is challenging, therefore additional work will be necessary to experimentally prove.

These AlphaFold3-based superpositions indicate that MinP-2 can competitively bind LCN2 by occupying binding sites shared with both MMP-9 and NGALR.

Conclusions

In this work, we demonstrated that a fully automated, AI-driven workflow – combining RFdiffusion for backbone creation, ProteinMPNN for sequence optimization, and AlphaFold2 for structure-based triage - can deliver potent miniproteins capable of binding LCN2 with high affinity.

From an initial library of 10,000 *in-silico* designs, five candidates were produced recombinantly, and one lead binder (MinP-2) displayed nanomolar affinity for LCN2 while maintaining high solubility and thermal stability. Furthermore, structural models suggest that binding is dominated by a short antiparallel β -augmentation interface, a motif that could be adapted or grafted onto other scaffolds to engineer new binders.

These findings establish a starting point for developing LCN2-targeted diagnostics or therapeutics that modulate neuroinflammatory pathways. Future work will focus on solving a high-resolution structure of the MinP-2–LCN2 complex and comprehensively evaluating the miniprotein's ability to disrupt pathological LCN2 interactions in cellular and *in-vivo* models. More broadly, our study underscores the power of generative deep-learning methods to accelerate ligand discovery for challenging protein–protein interfaces, even in the absence of prior binder templates.

Data availability statement

The raw data supporting the conclusions of this article will be made available by the authors, without undue reservation.

Author contributions

JS: Conceptualization, Investigation, Supervision, Writing – original draft, Writing – review & editing, Formal analysis, Validation. SB: Investigation, Writing – review & editing, Formal analysis, Validation, Writing – original draft. PL: Investigation,

Writing – review & editing, Writing – original draft. CG: Investigation, Supervision, Writing – review & editing, Writing – original draft. AF: Investigation, Writing – original draft, Writing – review & editing. YC: Investigation, Writing – review & editing. GZ: Investigation, Writing – review & editing. AC: Writing – review & editing, Conceptualization, Funding acquisition, Supervision, Writing – original draft.

Funding

The author(s) declare financial support was received for the research and/or publication of this article. This work was supported by the SNF grant CRSII—222762.

Conflict of interest

The authors declare that the research was conducted in the absence of any commercial or financial relationships that could be construed as a potential conflict of interest.

Generative AI statement

The author(s) declare that no Generative AI was used in the creation of this manuscript.

Any alternative text (alt text) provided alongside figures in this article has been generated by Frontiers with the support of artificial intelligence and reasonable efforts have been made to ensure accuracy, including review by the authors wherever possible. If you identify any issues, please contact us.

Publisher's note

All claims expressed in this article are solely those of the authors and do not necessarily represent those of their affiliated organizations, or those of the publisher, the editors and the reviewers. Any product that may be evaluated in this article, or claim that may be made by its manufacturer, is not guaranteed or endorsed by the publisher.

Supplementary material

The Supplementary Material for this article can be found online at: https://www.frontiersin.org/articles/10.3389/fimmu.2025. 1631868/full#supplementary-material

References

- 1. Chandrasekaran P, Weiskirchen S, Weiskirchen R. Structure, functions, and implications of selected lipocalins in human disease. *Int J Mol Sci.* (2024) 25:4290. doi: 10.3390/ijms25084290
- 2. Bao G, Clifton M, Hoette TM, Mori K, Deng SX, Qiu A, et al. Iron traffics in circulation bound to a siderocalin (Ngal)-catechol complex. *Nat Chem Biol.* (2010) 6, 602–609.
- 3. Chia WJ, Dawe GS, Ong WY. Expression and localization of the iron-siderophore binding protein lipocalin 2 in the normal rat brain and after kainate-induced excitotoxicity. *Neurochem Int.* (2011) 59:591–9. doi: 10.1016/j.neuint.2011.04.007
- 4. Jha MK, Lee S, Park DH, Kook H, Park KG, Lee IK, et al. Diverse functional roles of lipocalin-2 in the central nervous system. *Neurosci Biobehav Rev.* (2015) 49:135–56. doi: 10.1016/j.neubiorev.2014.12.006
- 5. Shao S, Cao T, Jin L, Li B, Fang H, Zhang J, et al. Increased lipocalin-2 contributes to the pathogenesis of psoriasis by modulating neutrophil chemotaxis and cytokine secretion. *J Invest Dermatol.* (2016) 136:1418–28. doi: 10.1016/j.jid.2016.03.002
- 6. Afridi R, Kim JH, Bhusal A, Lee WH, Suk K. Lipocalin-2 as a mediator of neuroimmune communication. *J Leukoc Biol.* (2024) 116:357–68. doi: 10.1093/jleuko/
- 7. Triebel S, Bläser J, Reinke H, Tschesche H. A 25 kDa alpha 2-microglobulin-related protein is a component of the 125 kDa form of human gelatinase. *FEBS Lett* (1992) 314, 386–388.
- 8. Kjeldsen I., Johnsen AH, Sengeløv H, Borregaard N. Isolation and primary structure of NGAL, a novel protein associated with human neutrophil gelatinase. *J Biol Chem* (1993) 268:10425–10432.
- 9. Jung BK, Ryu KY. Lipocalin-2: a therapeutic target to overcome neurodegenerative diseases by regulating reactive astrogliosis. *Exp Mol Med.* (2023) 55:2138–46. doi: 10.1038/s12276-023-01098-7
- 10. Ram M, Sherer Y, Shoenfeld Y. Matrix metalloproteinase-9 and autoimmune diseases. J Clin Immunol. (2006) 26:299–307. doi: 10.1007/s10875-006-9022-6
- 11. Shigemori Y, Katayama Y, Mori T, Maeda T, Kawamata T. Matrix metalloproteinase-9 is associated with blood-brain barrier opening and brain edema formation after cortical contusion in rats. *Acta Neurochir Suppl.* (2006) 96:130–3. doi: 10.1007/3-211-30714-1_29
- 12. Vafadari B, Salamian A, Kaczmarek L. MMP-9 in translation: from molecule to brain physiology, pathology, and therapy. J Neurochem. (2016) 139:91–114. doi: 10.1111/jnc.13415
- 13. Bae JS, Heo JE, Ryu KY. Proteasome inhibition suppresses the induction of lipocalin-2 upon systemic lipopolysaccharide challenge in mice. *Mol Brain.* (2024) 17:73. doi: 10.1186/s13041-024-01147-w
- 14. Qiu R, Cai Y, Su Y, Fan K, Sun Z, Zhang Y. Emerging insights into Lipocalin-2: Unraveling its role in Parkinson's Disease. *Biomed Pharmacother*. (2024) 177:116947. doi: 10.1016/j.biopha.2024.116947

- 15. Nada H, Choi Y, Kim S, Jeong KS, Meanwell NA, Lee K. New insights into protein-protein interaction modulators in drug discovery and therapeutic advance. *Signal Transduct Target Ther.* (2024) 9:341. doi: 10.1038/s41392-024-02036-3
- 16. Cao L, Goreshnik I, Coventry B, Case JB, Miller L, Kozodoy L, et al. *De novo* design of picomolar SARS-CoV-2 miniprotein inhibitors. *Sci (New York N.Y.).* (2020) 370:426–31. doi: 10.1126/science.abd9909
- 17. Huang B, Coventry B, Borowska MT, Arhontoulis DC, Exposit M, Abedi M, et al. *De novo* design of miniprotein antagonists of cytokine storm inducers. *Nat Commun.* (2024) 15:7064. doi: 10.1038/s41467-024-50919-4
- 18. Weinberg ZY, Soliman SS, Kim MS, Shah DH, Chen IP, Ott M, et al. *De novo*-designed minibinders expand the synthetic biology sensing repertoire. *bioRxiv*. (2024) 13:RP96154. doi: 10.7554/eLife.96154.1
- 19. Yang W, Hicks DR, Ghosh A, Schwartze TA, Conventry B, Goreshnik I, et al. Design of high-affinity binders to immune modulating receptors for cancer immunotherapy. *Nat Commun.* (2025) 16:2001. doi: 10.1038/s41467-025-57192-z
- 20. Watson JL, Juergens D, Bennett NR, Trippe BL, Yim J, Eisenach HE, et al. *De novo* design of protein structure and function with RFdiffusion. *Nature*. (2023) 620:1089–100. doi: 10.1038/s41586-023-06415-8
- 21. Goetz DH, Willie ST, Armen RS, Bratt T, Borregaard N, Strong RK. Ligand preference inferred from the structure of neutrophil gelatinase associated lipocalin. *Biochemistry.* (2000) 39:1935–41. doi: 10.1021/bi992215v
- 22. Dauparas J, Anishchenko I, Bennett N, Bai H, Ragotte RJ, Milles LF, et al. Robust deep learning-based protein sequence design using ProteinMPNN. *Sci (New York N.Y.)*. (2022) 378:49–56. doi: 10.1126/science.add2187
- 23. Jumper J, Evans R, Pritzel A, Green T, Figurnov M, Ronneberger O, et al. Highly accurate protein structure prediction with AlphaFold. *Nature*. (2021) 596:583–9. doi: 10.1038/s41586-021-03819-2
- 24. Vangone A, Bonvin A. PRODIGY: A contact-based predictor of binding affinity in protein-protein complexes. *Bio Protoc.* (2017) 7:e2124. doi: 10.21769/BioProtoc.2124
- 25. Kruger DM, Gohlke H. DrugScorePPI webserver: fast and accurate in silico alanine scanning for scoring protein-protein interactions. *Nucleic Acids Res.* (2010) 38: W480–486. doi: 10.1093/nar/gkq471
- 26. Bennett NR, Coventry B, Goreshnik I, Huang B, Allen A, Vafeados D, et al. Improving *de novo* protein binder design with deep learning. *Nat Commun.* (2023) 14:2625. doi: 10.1038/s41467-023-38328-5
- 27. Vázquez Torres S, Leung PJY, Venkatesh P, Lutz ID, Hink F, Huynh HH, et al. De novo design of high-affinity binders of bioactive helical peptides. *Nature*. (2024) 626, 435–442.
- 28. Cao L, Coventry B, Goreshnik I, Huang B, Sheffler W, Park JS, et al. Design of protein-binding proteins from the target structure alone. *Nature*. (2022) 605:551–60. doi: 10.1038/s41586-022-04654-9